Purdue University
Purdue e-Pubs

Department of Electrical and Computer Engineering Faculty Publications

Department of Electrical and Computer Engineering

2013

A computational study of the thermoelectric performance of ultrathin Bi2Te3 films

Jesse Maassen
Birck Nanotechnology Center, Purdue University, jmaassen@purdue.edu

Mark S. Lundstrom
Purdue University, lundstro@purdue.edu

Follow this and additional works at: https://docs.lib.purdue.edu/ecepubs

Part of the Electrical and Computer Engineering Commons

Maassen, Jesse and Lundstrom, Mark S., "A computational study of the thermoelectric performance of ultrathin Bi2Te3 films" (2013). *Department of Electrical and Computer Engineering Faculty Publications.* Paper 147.
https://docs.lib.purdue.edu/ecepubs/147

This document has been made available through Purdue e-Pubs, a service of the Purdue University Libraries. Please contact epubs@purdue.edu for additional information.

A computational study of the thermoelectric performance of ultrathin Bi_2Te_3 films

Jesse Maassen[a)] and Mark Lundstrom
Network for Computational Nanotechnology, School of Electrical and Computer Engineering, Purdue University, West Lafayette, Indiana 47907, USA

(Received 18 September 2012; accepted 22 February 2013; published online 4 March 2013)

The ballistic thermoelectric performance of ultrathin films of Bi_2Te_3, ranging in thickness from 1 to 6 quintuple layers, is analyzed using density functional theory combined with the Landauer approach. Our results show that the thinnest film, corresponding to a single quintuple layer, has an intrinsic advantage originating from the particular shape of its valence band, leading to a large power factor and figure-of-merit exceeding bulk Bi_2Te_3. The interaction between the top and bottom topological surface states is key. The thinnest film yields a six-fold increase in power factor compared to bulk. © *2013 American Institute of Physics*. [http://dx.doi.org/10.1063/1.4794534]

A key goal of thermoelectric (TE) research is increasing the material figure-of-merit ZT, which is directly related to the efficiency of the thermal/electrical energy conversion. The figure-of-merit is expressed as $ZT = S^2GT/(K_e + K_l)$, where S is the Seebeck coefficient, G is the electrical conductance, T is the temperature, and $K_{e/l}$ is the electronic/lattice thermal conductance.[1–6] Recent theoretical works have suggested that very thin films ($\sim$1 nm) of Bi_2Te_3 and/or Bi_2Se_3 may yield enhanced in-plane ZT values, exceeding that of bulk.[7,8] According to Refs. 7 and 8, the interaction between the top and bottom surface states of these topological insulators (TI)[9] is responsible for this potential gain in ZT. In general, improvements in ZT occur in two ways: by a reduction in thermal conductance or by an enhancement of the product S^2G known as the power factor (PF). With regard to the former strategy, the use of nano-engineered structures has proven effective in suppressing heat conduction.[10] It has proven more difficult to enhance the electrical performance, but this is believed to be necessary for continued progress,[11] and recent experiments show promise.[12] Interestingly, the proposed improvement in ZT with ultrathin TI films is via the PF. Understanding the source of this improvement may point the way towards higher TE efficiencies.

In this study, we wish to understand the source of the potential PF enhancement in ultrathin Bi_2Te_3 and/or Bi_2Se_3 and how the TE performance of these films varies with thickness. Utilizing first principles calculations combined with the Landauer transport formalism, our findings confirm that a 1 quintuple layer (QL)-thick film is a superior TE compared to bulk Bi_2Te_3. An enhanced PF stems from the unique shape of the valence band that is very unlike parabolic dispersion. A strict constraint on thickness (t) is found because all the studied films ($t = 0.74$ nm to 5.82 nm) thicker than 1 QL compared worse than bulk. Bulk properties are retrieved when t is large enough such that conduction through the TI surface states becomes negligible.

Bulk Bi_2Te_3 has a rhombohedral crystal structure, which along the c-axis can be viewed as stacked 5-atom-thick layers called quintuple layers. A single QL has the sequence Te_1-Bi-Te_2-Bi-Te_1 of atoms along its thickness, where Te_1 and Te_2 are inequivalent. Within a QL the chemical bonds are strong whereas the van der Waals-type interaction connecting different QLs is weak. Thus, Bi_2Te_3 films can be mechanically exfoliated or cleaved[13] or atomically grown[14] and are likely to have a thickness corresponding to an integer number of QLs. The bare surfaces of Bi_2Te_3 films do not have dangling bonds and thus do not require chemical passivation. However, exposure to atmospheric conditions can lead to surface oxidation, which electron dopes the surface but does not destroy the topological surface states.[15] The films have a hexagonal crystal structure defined by the length of the two in-plane and one cross-plane lattice vectors, $a = 4.38$ Å and $c = 30.49$ Å, with values taken from bulk,[16] as previously done.[17]

The electronic structure of bulk and ultrathin film Bi_2Te_3 is computed using density functional theory (DFT). Fig. 1 presents the two-dimensional (2D) band structure of Bi_2Te_3 films, with thickness t ranging from 1 QL (0.74 nm) to 5 QL (4.81 nm) [6 QL (5.82 nm) not shown]. The calculations were performed using the VASP simulation package,[18] the generalized gradient approximation[19] for the exchange-correlation potential and including spin-orbit interaction (further computational details can be found here[20]). Fig. 1 shows that only 1 QL and 2 QL films possess a band gap (indirect) of 0.268 eV and 0.050 eV, respectively, resulting from the interaction between the top and bottom TI surface states. For QL ≥ 3, the surface states decay exponentially in the insulating bulk effectively suppressing any interaction and closing the band gap, consistent with the previous reports.[17,21] Since a band gap is generally desirable for a large Seebeck coefficient, the TE properties of these films are expected to have a strong thickness dependence.

The thermoelectric coefficients can be expressed as[22]

$$G = \int_{-\infty}^{\infty} G'(\epsilon)\, d\epsilon, \tag{1}$$

$$S = -\frac{k_B}{q}\int_{-\infty}^{\infty}\left(\frac{\epsilon - E_F}{k_BT}\right)\frac{G'(\epsilon)}{G}\, d\epsilon, \tag{2}$$

[a)]Electronic mail: jmaassen@purdue.edu.

 © 2013 American Institute of Physics

Reuse of AIP Publishing content is subject to the terms at: https://publishing.aip.org/authors/rights-and-permissions. Download to IP: 128.210.106.225 On: Thu, 08 Dec 2016 14:43:13

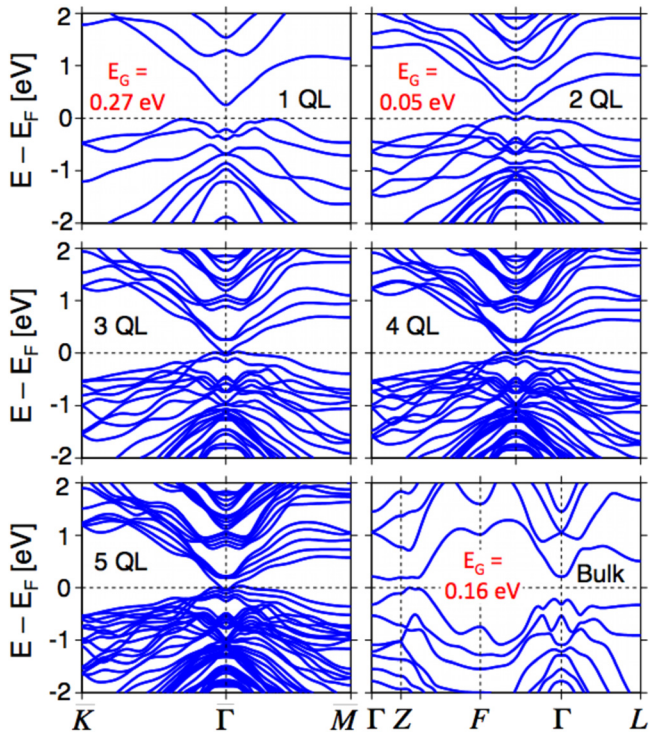

FIG. 1. DFT-computed electronic structure of Bi_2Te_3 films with t equal to 1 QL (0.74 nm), 2 QL (1.76 nm), 3 QL (2.77 nm), 4 QL (3.79 nm), 5 QL (4.81 nm), and bulk. 1 QL, 2 QL, and bulk have indirect band gaps (E_G) of 0.268 eV, 0.050 eV, and 0.16 eV (bulk E_G adjusted to the experimental value). For $t \geq 3$ QL, the band gap closes due to the surface states. Bulk calculations correspond to an infinite solid, and hence no surface states are present. In practice, if the bulk is not perfectly insulating, the surface states would contribute negligibly to bulk samples.

$$K_0 = \left(\frac{k_B}{q}\right)^2 T \int_{-\infty}^{\infty} \left(\frac{\epsilon - E_F}{k_B T}\right)^2 G'(\epsilon)\, d\epsilon, \tag{3}$$

where $G'(\epsilon)$ is the differential conductance, E_F is the Fermi level, k_B is Boltzmann's constant, q is the electron charge, T is the temperature, and K_0 is the zero-electric-field (closed circuit) electronic thermal conductance. The open circuit electronic thermal conductance K_e is extracted using the relation $K_e = K_0 - S^2 GT$. The central quantity in determining the TE parameters is $G'(\epsilon)$, which in the Landauer picture is written as[22]

$$G'(\epsilon) = \frac{2q^2}{h} M(\epsilon)\, T(\epsilon) \left[-\frac{\partial f}{\partial \epsilon}\right], \tag{4}$$

where $M(\epsilon)$ is the distribution of modes (DOM), $T(\epsilon)$ is the transmission coefficient, f is the Fermi occupation function, and h is Planck's constant. The term $-\partial f/\partial \epsilon$ is symmetric, centered around E_F, and decays exponentially; thus, the above integrals are safely evaluated in the range $E_F \pm 15\, k_B T$. In this work, we compute the ballistic TE properties $T(\epsilon) = 1$, which depend only on band structure, and hence assess a material's inherent potential as a good TE. Note that $M(\epsilon)$ corresponds to the number of quantum conducting channels and is proportional to the average velocity along the transport direction z times the density of states: $M(\epsilon) \propto \langle |v_z(\epsilon)| \rangle \cdot D(\epsilon)$. The DOM is extracted from the electronic dispersion of any system using[22]

$$M(\epsilon) = \left(\frac{L_\perp}{2\pi}\right)^{d-1} \int_{BZ} \sum_{n^+} \Theta(\epsilon - \epsilon_{k_\perp})\, dk_\perp^{d-1}, \tag{5}$$

where d is the dimensionality of the system, $L_\perp$ is the length of the sample in the direction perpendicular to transport [$L_\perp^2 = W \times t$ for $d = 3$ and $L_\perp = W$ for $d = 2$; W: width, t: thickness], $\Theta(\epsilon)$ is a unit step function, $k_\perp$ is the reciprocal lattice vector in the plane perpendicular to transport, and n^+ corresponds to the number of positive velocity states with energy ϵ at $k_\perp$. The above equation describes the fact that one forward moving band ($\partial \epsilon_k / \partial k_z > 0$) provides one conducting channel. For a parabolic band, the bulk three-dimensional (3D) and film 2D DOM are $M_{3D} = W t m^* \epsilon / 2\pi\hbar^2$ and $M_{2D} = W\sqrt{2m^*\epsilon}/\pi\hbar$, where m^* is the effective mass.[5]

Fig. 2 shows the DOM versus energy for bulk and ultrathin films of Bi_2Te_3. The analytical electronic dispersion model in Ref. 8 is also plotted, where $M(\epsilon) = \sqrt{\epsilon^2 - \Delta^2}/(\pi v_D \hbar)$ (fitting our 1 QL data we find $\Delta = 134$ meV and $v_D = 5 \times 10^5$ m/s, where 2Δ is the band gap and v_D is the constant band velocity when $\Delta = 0$). E_F corresponds to the self-consistently calculated Fermi level, which is the valence band (VB) edge for semiconductors. The DOM of 1 QL is noticeably different from 2 QL, 3 QL, and bulk; with 1 QL showing a sharp, discrete-like increase in DOM at the VB edge while the other curves show gradual increases. As will be shown, this feature is advantageous for increasing PF because G is enhanced near the VB edge. The DOM of films with $t \geq 4$ QL are very similar to 3 QL and are not presented for clarity. We note that the shapes of the DOM for 1 QL and bulk are consistent with a previous report; however, a difference in magnitude is observed[7] which can be partly explained by a spin degeneracy factor of 2 (not included in our definition of $M(\epsilon)$).

Next, we examine the TE properties. The Seebeck (S) coefficient versus E_F is shown in Fig. 3(a). The maximum positive S (p-type transport) occurs with 1 QL near mid-gap with S approaching 500 μV/K; however, the most negative S (n-type transport) occurs with bulk Bi_2Te_3. The large DOM

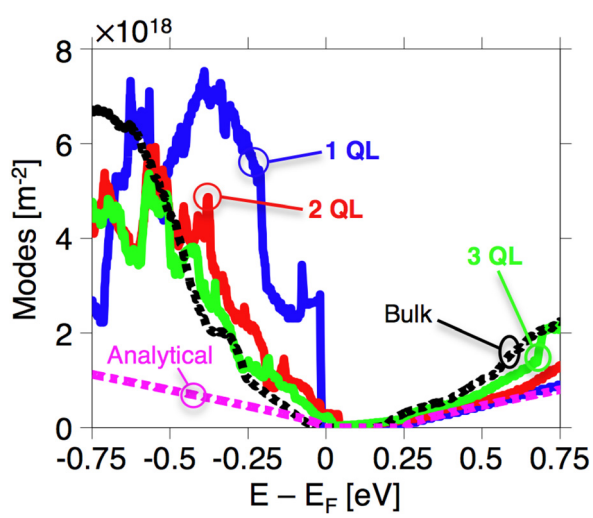

FIG. 2. Distribution of modes versus energy for 1 QL, 2 QL, 3 QL, bulk Bi_2Te_3, and the analytical model in Ref. 8 (fitting our 1 QL data: $\Delta = 134$ meV and $v_D = 5 \times 10^5$ m/s). The DOM for films is divided by the thickness t to compare to bulk. Transport is along Γ-K (binary axis) and is found to be identical to transport along Γ-M (bisectrix axis).

Reuse of AIP Publishing content is subject to the terms at: https://publishing.aip.org/authors/rights-and-permissions. Download to IP: 128.210.106.225 On: Thu, 08 Dec 2016 14:43:13

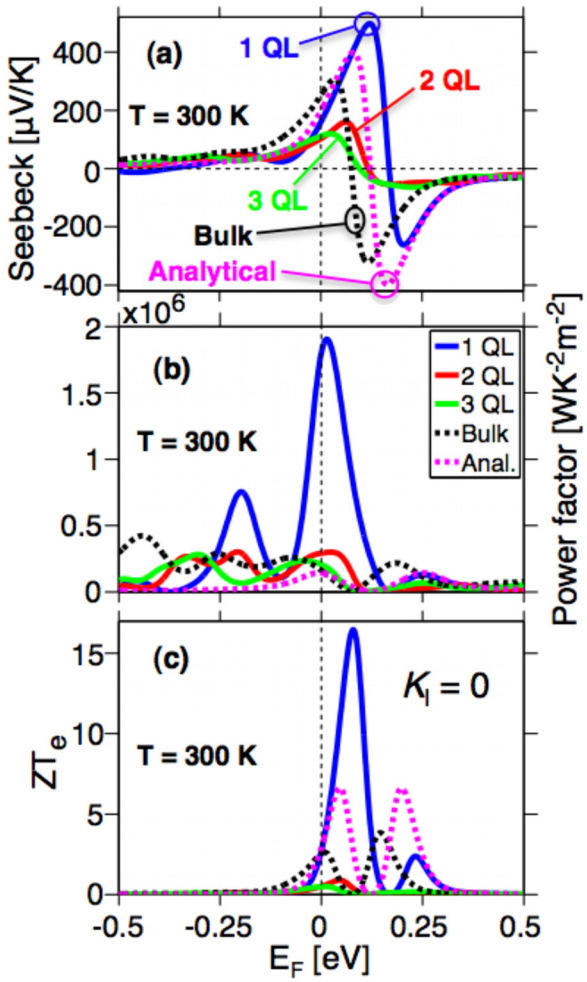

FIG. 3. Seebeck coefficient (a), power factor (b), and electronic ZT (ZT_e) (c) versus Fermi level (E_F) at $T = 300$ K for 1 QL, 2 QL, 3 QL, bulk Bi_2Te_3, and the analytical model in Ref. 8. Electronic ZT is obtained by assuming $K_l = 0$ in the expression of figure-of-merit. Note that the units of power factor are different in the ballistic and diffusive transport regimes. Assuming a constant mean-free-path, the diffusive power factor (units of W/K^2m) is obtained by simply multiplying the results in (b) by the mean-free-path.

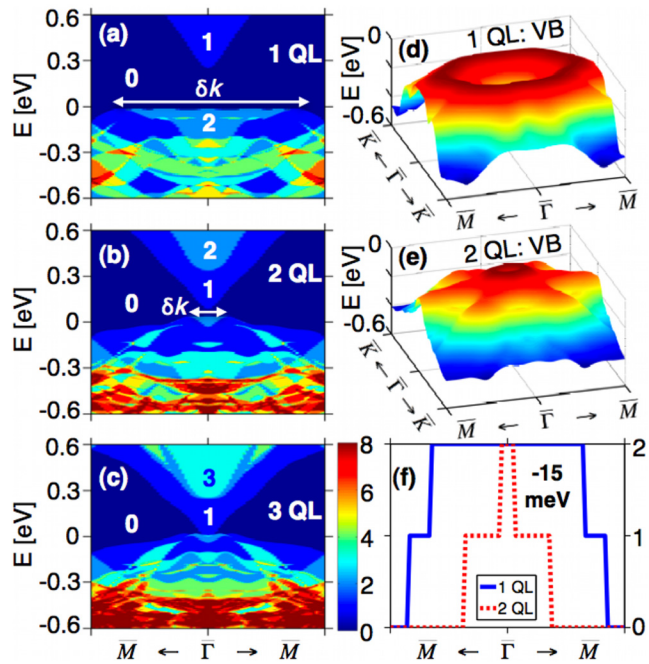

FIG. 4. (a)–(c) $k_\perp$-resolved DOM (integrand of Eq. (5)) versus energy for 1 QL, 2 QL, and 3 QL. Each color corresponds to an integer value equal to the number of conducting channels at a given $k_\perp$. (d)–(e) Surface plot of the VB for 1 QL and 2 QL, showing how the VB of 1 QL is pushed downward near Γ. (f) Line plot taken from (a) and (b) at an energy of −15 meV below the VB edge. Note that the DOM shown in Fig. 2 is proportional to the integral of these curves divided by t.

at the VB edge is the reason why S is not anti-symmetric as is the case with the analytical model. Our simulations indicate that S decreases with increasing thickness, the result of a shrinking band gap. Physically, S is equal to the average energy (relative to E_F) at which current flows times $-k_B/q$; thus, a large $|S|$ requires a large asymmetry between electron and hole conduction. With a band gap, one can vary E_F such that the average conduction energy is located far above (n-type) or below (p-type) E_F, thus yielding a large $|S|$. With metals, conduction above and below E_F is roughly equal, leading to a small $|S|$. Note that S initially drops due to the closing of the band gap by the TI surface states, but as the thickness increases conduction through the bulk will eventually dominate thus allowing S to retrieve its bulk value. With 1 QL, S is large because: (i) the band gap is larger than bulk and (ii) the large asymmetry in the VB and the conduction band (CB) DOM means that S continues growing until midgap before changing sign. We highlight that such features can easily be found in many semiconductors and that 1 QL Bi_2Te_3 is not special in regard to the Seebeck coefficient.

Fig. 3(b) shows the ballistic power factor ($PF = S^2G$) versus E_F. One QL shows a maximum PF that is more than 6× larger than all other materials. This enhancement in PF originates from G and not S; in fact, the S value at the optimal PF is smaller with 1 QL than bulk. It is the sharp increase in DOM, shown in Fig. 2, that dramatically increases G near the VB edge. Contrary to the increase in S, PF is enhanced due to the unique electronic dispersion of 1 QL Bi_2Te_3. Fig. 3(c) presents the electronic ZT (ZT_e), which corresponds to assuming the lattice thermal conductance is zero: S^2G/K_e. To calculate ZT, knowledge of the lattice thermal conductance extracted from phonon transport is required, which is also expected to vary with the number of QLs. Assuming the ballistic lattice thermal conductance of bulk, the relative contribution of the electronic thermal conductance for 1 QL, 2 QL, and 3 QL is found to be roughly 50% near $E_F = 0$ and increases as E_F moves further into the valence or conduction band. In reality, ZT will always be smaller with a finite value of K_l; however, Fig. 3(c) allows us to compare the electronic component of ZT in each material. One QL demonstrates a ZT_e that is ∼5× greater than bulk. Films ≥ 2 QL are worse compared to bulk because of their low S and high K_e arising from a small or zero band gap. We emphasize that with 1 QL the enhancement in ZT_e, via PF, stems from the particular electronic character of this material and not a reduction in lattice thermal conductance.

Next, we wish to understand what is special with 1 QL, which results in the rapid increase in DOM and enhances PF and ZT_e. For this purpose, we plot the $k_\perp$-resolved DOM versus energy for 1 QL, 2 QL, and 3 QL in Figs. 4(a)–4(c). The $k_\perp$-DOM corresponds to the integrand of Eq. (5), where each color represents an integer equal to the number of quantum conducting channels. The surface states are easily identified

Reuse of AIP Publishing content is subject to the terms at: https://publishing.aip.org/authors/rights-and-permissions. Download to IP: 128.210.106.225 On: Thu, 08 Dec 2016 14:43:13

because they provide a fixed number of modes independent of t. The sharp increase in DOM with 1 QL occurs since the width δk, in $k_\perp$-space (along Γ-M), corresponding to the region where the modes are non-zero discretely jumps from zero (in the band gap) to almost the whole Brillouin zone at the VB edge. This feature is unlike what is observed with 2–3 QL or parabolic-type dispersions, where δk (and the DOM) smoothly increases from the band edge. According to Eq. (5), $M(\epsilon)$ depends on the integral of $k_\perp$-DOM at a fixed ϵ. As an example, in panel (f) we plot $k_\perp$-DOM at the energy $\epsilon = -15$ meV, where the area under the curve is clearly larger for 1 QL than 2 QL. This feature in the $k_\perp$-DOM that is responsible for the discrete increase in DOM is directly related to the particular shape of the VB: the VBs of 1 QL and 2 QL are shown in Figs. 4(d) and 4(e). With 1 QL, the interaction between top/bottom surface states pushes down the VB of 1 QL near Γ. This indented shape of the VB, not observed with 2 QL (or thicker films), is what leads to the unique TE properties of 1 QL Bi_2Te_3.

Lastly, we consider whether scattering will hinder the predicted TE properties of 1 QL. In the diffusive limit, the transmission scales as $T(\epsilon) \propto \langle |v_z(\epsilon)| \rangle \tau(\epsilon)/L$,[22] where $\tau(\epsilon)$ is the scattering time. Ideally, we wish for the product $\langle |v_z(\epsilon)| \rangle \tau(\epsilon)$ to be large. The scattering time $\tau(\epsilon)$ depends on the particular scattering physics and is difficult to accurately compute whereas $\langle |v_z(\epsilon)| \rangle$ is extracted from the electronic dispersion. Here, we do not attempt to calculate $\tau(\epsilon)$, but we find $\langle |v_z(\epsilon)| \rangle > 10^5$ m/s near the VB (comparable to bulk Bi_2Te_3), thus indicating that the carrier velocity itself should not be a limiting factor.

In conclusion, by analyzing the ballistic thermoelectric properties of ultrathin Bi_2Te_3 films, ranging in thickness from 1 QL to 6 QL, we determined that only the thinnest film shows a large enhancement in power factor and ZT_e, compared to bulk. This result is traced back to (i) the opening of a sizeable band gap with 1 QL and (ii) the unique indented shape of the 1 QL valence band, which we propose is intrinsically advantageous for achieving a large PF. This particular band shape, distinct from the parabolic dispersion found in most semiconductors, shares similarities with Rashba/Dresselhaus-type bands but without spin-splitting such as the model used in Ref. 23. Useful applications will likely require stacking these ultrathin films for achieving high PF. Perhaps, an alternative route towards high efficiency/performance thermoelectric applications involves understanding, finding, and designing *bulk* materials with similar band shapes.

We acknowledge DARPA MESO (No. N66001-11-1-4107) for financial support and the Network for Computational Nanotechnology and Professor Hong Guo (J. M.) for providing computational resources.

[1]A. Majumdar, Science **303**, 777 (2004).
[2]T. M. Tritt, Science **283**, 804 (1999).
[3]C. Jeong, S. Datta, and M. Lundstrom, J. Appl. Phys. **109**, 073718 (2011).
[4]L. D. Hicks and M. S. Dresselhaus, Phys. Rev. B **47**, 16631 (1993); L. D. Hicks and M. S. Dresselhaus, *ibid.* **47**, 12727 (1993).
[5]R. Kim, S. Datta, and M. S. Lundstrom, J. Appl. Phys. **105**, 034506 (2009).
[6]R. Venkatasubramanian, E. Siivola, T. Colpitts, and B. O'Quinn, Nature (London) **413**, 597 (2001).
[7]F. Zahid and R. Lake, Appl. Phys. Lett. **97**, 212102 (2010).
[8]P. Ghaemi, R. S. K. Mong, and J. E. Moore, Phys. Rev. Lett. **105**, 166603 (2010).
[9]H. Zhang, C.-X. Liu, X.-L. Qi, X. Dai, Z. Fang, and S.-C. Zhang, Nat. Phys. **5**, 438 (2009).
[10]W. Kim, J. Zide, A. Gossard, D. Klenov, S. Stemmer, A. Shakouri, and A. Majumdar, Phys. Rev. Lett. **96**, 045901 (2006); B. Poudel, Q. Hao, Y. Ma, Y. Lan, A. Minnich, B. Yu, X. Yan, D. Wang, A. Muto, D. Vashaee *et al.*, Science **320**, 634 (2008); A. I. Hochbaum, R. Chen, R. D. Delgado, W. Liang, E. C. Garnett, M. Najarian, A. Majumdar, and P. Yang, Nature (London) **451**, 163 (2008).
[11]A. J. Minnich, M. S. Dresselhaus, Z. F. Ren, and G. Chen, Energy Environ. Sci. **2**, 466 (2009); M. Zebarjadi, K. Esfarjani, M. S. Dresselhaus, Z. F. Ren, and G. Chen, Energy Environ. Sci. **5**, 5147 (2012).
[12]J. P. Heremans, V. Jovovic, E. S. Toberer, A. Saramat, K. Kurosaki, A. Charoenphakdee, S. Yamanaka, and G. J. Snyder, Science **321**, 554 (2008); Y. Pei, X. Shi, A. LaLonde, H. Wang, L. Chen, and G. J. Snyder, Nature (London) **473**, 66 (2011).
[13]D. Teweldebrhan, V. Goyal, and A. A. Balandin, Nano Lett. **10**, 1209 (2010).
[14]R. Venkatasubramanian, T. Colpitts, E. Watko, M. Lamvik, and N. El-Masry, J. Cryst. Growth **170**, 817 (1997); Y.-Y. Li, G. Wang, X.-G. Zhu, M.-H. Liu, C. Ye, X. Chen, Y.-Y. Wang, K. He, L.-L. Wang, X.-C. Ma *et al.*, Adv. Mater. **22**, 4002 (2010).
[15]C. Chen, S. He, H. Weng, W. Zhang, L. Zhao, H. Liu, X. Jia, D. Mou, S. Liu, J. He *et al.*, Proc. Natl. Acad. Sci. **109**, 3694 (2012).
[16]W. Zhang, R. Yu, H.-J. Zhang, X. Dai, and Z. Fang, New J. Phys. **12**, 065013 (2010).
[17]O. V. Yazyev, J. E. Moore, and S. G. Louie, Phys. Rev. Lett. **105**, 266806 (2010).
[18]G. Kresse and J. Furthmuller, Phys. Rev. B **54**, 11169 (1996); Comput. Mater. Sci. **6**, 15 (1996).
[19]J. P. Perdew, K. Burke, and M. Ernzerhof, Phys. Rev. Lett. **77**, 3865 (1996).
[20]A plane-wave energy cutoff of (300 eV: films, 250 eV: bulk) was used, and the core was treated using the projector augmented wave method. The self-consistent calculations used a k-mesh of (11×11: films, $9 \times 9 \times 9$: bulk) generated using the Monkhorst-Pack scheme. A total of (19550: films, 384750: bulk) k-points were used to sample the Brillouin zone when calculating the distribution of modes.
[21]Y. Zhao, Y. Hu, L. Liu, Y. Zhu, and H. Guo, Nano Lett. **11**, 2088 (2011).
[22]C. Jeong, R. Kim, M. Luisier, S. Datta, and M. Lundstrom, J. Appl. Phys. **107**, 023707 (2010).
[23]Y. Zhang, K. He, C.-Z. Chang, C.-L. Song, L.-L. Wang, X. Chen, J.-F. Jia, Z. Fang, X. Dai, W.-Y. Shan *et al.*, Nat. Phys. **6**, 584 (2010).

Reuse of AIP Publishing content is subject to the terms at: https://publishing.aip.org/authors/rights-and-permissions. Download to IP: 128.210.106.225 On: Thu, 08 Dec 2016 14:43:13

AIP Applied Physics Letters

A computational study of the thermoelectric performance of ultrathin Bi2Te3 films

Jesse Maassen and Mark Lundstrom

Citation: Applied Physics Letters **102**, 093103 (2013); doi: 10.1063/1.4794534
View online: http://dx.doi.org/10.1063/1.4794534
View Table of Contents: http://scitation.aip.org/content/aip/journal/apl/102/9?ver=pdfcov
Published by the AIP Publishing

Articles you may be interested in

Origins of enhanced thermoelectric power factor in topologically insulating Bi0.64Sb1.36Te3 thin films
Appl. Phys. Lett. **108**, 043902 (2016); 10.1063/1.4940923

Theoretical and experimental investigations of the thermoelectric properties of Bi2S3
J. Appl. Phys. **117**, 125103 (2015); 10.1063/1.4916528

Thermoelectric properties of topological insulator Bi2Te3, Sb2Te3, and Bi2Se3 thin film quantum wells
Appl. Phys. Lett. **105**, 123117 (2014); 10.1063/1.4896680

Crossover between two-dimensional surface state and three-dimensional bulk phase in Fe-doped Bi2Te3
Appl. Phys. Lett. **104**, 252413 (2014); 10.1063/1.4885148

Topological insulator Bi2Te3 films synthesized by metal organic chemical vapor deposition
Appl. Phys. Lett. **101**, 162104 (2012); 10.1063/1.4760226

Reuse of AIP Publishing content is subject to the terms at: https://publishing.aip.org/authors/rights-and-permissions. Download to IP: 128.210.106.225 On: Thu, 08 Dec 2016 14:43:13